Ionics (2018) 24:3075–3084
https://doi.org/10.1007/s11581-017-2427-9

ORIGINAL PAPER

Microwave-sintered Pr^{3+}, Sm^{3+}, and Gd^{3+} triple-doped ceria electrolyte material for IT-SOFC applications

Kasarapu Venkataramana[1] · Chittimadula Madhuri[1] · Jada Shanker[1] · Ch. Madhusudan[1] · C. Vishnuvardhan Reddy[1]

Received: 17 November 2017 / Revised: 23 December 2017 / Accepted: 26 December 2017 / Published online: 4 January 2018

Abstract
The Pr^{3+}, Sm^{3+}, and Gd^{3+} triple-doped ceria $Ce_{0.76}Pr_{0.08}Sm_{0.08}Gd_{0.08}O_{2-\delta}$ material as solid electrolyte for IT-SOFC has been successfully synthesized by sol–gel auto-combustion route. The effect of microwave sintering (1300 °C for 15, 30, and 60 min, named as PSG-MS15, PSG-MS30, and PSG-MS60, respectively) on structural, electrical, and thermal properties of prepared electrolyte material has been studied. Powder X-ray diffraction, scanning electron microscope, energy dispersive spectroscopy, and Raman analysis revealed the single phase, microstructure, elemental confirmation, and structural oxygen vacancy formation of all the samples. Impedance spectroscopy analysis revealed the highest total ionic conductivity, i.e., 3.47×10^{-2} S cm^{-1} at 600 °C with minimum activation energy of 0.69 eV, in PSG-MS30 sample when compared to PSG-MS15 and PSG-MS60. The thermal expansion measurements have been carried out for PSG-MS30 specimen. The highest total ionic conductivity with minimum activation energy and moderate thermal expansion coefficient of PSG-MS30 sample makes the possibility of its use as solid electrolyte in IT-SOFC applications.

Keywords Triple-doped ceria · Solid electrolyte · Microwave sintering · Total ionic conductivity · IT-SOFC

Introduction

Among the various fuel cell technologies, solid oxide fuel cell (SOFC) has proved as more efficient and best promising electrochemical energy conversion technology, in which the chemical energy in the form of fuel is converted into electricity with high efficiency. SOFCs have a great interest due to its clean environment-friendly energy conversion, in which only heat and water are produced as byproducts [1]. Solid electrolyte material plays a tremendous role in the SOFC system by facilitating the mobilization of ions from anode to cathode in order to increase the performance of the cell. Therefore, solid electrolyte should exhibit high ionic conductivity to enhance the performance of SOFC [2]. Zirconia-based solid electrolytes exhibit the highest ionic conductivity at higher temperatures (above 800 °C). However, at such high temperatures, there is a significant decrease in the output efficiency of SOFC which may lead to short circuit [3]. Extended investigations have been made on doped ceria solid electrolytes due to their improved performance and reduced operating temperature to intermediate range (i.e., 600–800 °C) over traditional zirconia-based electrolytes in order to develop intermediate temperature solid oxide fuel cells [3, 4]. However, the single-doped ceria electrolyte materials are facing some difficulties due to the reduction of ceria in reducing environment and the growth of defect clusters in the ceria structure which results in lower ionic conductivity [5–7]. To overcome these problems, further doping in ceria is required. In the past few decades, plenty of research has been made on co-doped ceria which exhibits the superior properties compared to single-doped ceria [5–12]. Anderson et al. [13] have investigated the relation between the lanthanide dopants and structural oxygen vacancies using density

Highlights
- The microwave sintered $Ce_{0.76}Pr_{0.08}Sm_{0.08}Gd_{0.08}O_{2-\delta}$ (PSG) solid electrolyte has been investigated for the first time.
- Effect of microwave sintering on structural, electrical, and thermal properties has been studied and compared.
- Influence of oxygen vacancy concentration on total ionic conductivity is investigated.
- Microwave-sintered sample PSG-MS30 exhibits the highest total ionic conductivity with moderate thermal expansion coefficient.
- This makes PSG-MS30 as a potential candidate for solid electrolyte in IT-SOFC applications.

✉ Kasarapu Venkataramana
kvrgoud56@gmail.com

[1] Department of Physics, Osmania University, Hyderabad, Telangana 500007, India

functional theory (DFT) and reported that the dopant with an effective atomic number between 61 (Pm^{3+}) and 62 (Sm^{3+}) is an optimized dopant in order to enhance the electrical properties of ceria. Unfortunately, Pm^{3+} is not suitable/useful for required applications. Therefore, this theory recommends that the dopants which are having an average atomic number close to Pm^{3+} and Sm^{3+} result in enhanced electrical properties [13]. Recently, Ramesh et al. [10], Rai et al. [14], Anirban et al. [15], Babu et al. [16], and Venkataramana et al. [17] have extensively investigated ceria-based solid electrolytes using DFT theory, such as $Ce_{1-x}(Gd_{0.5}Pr_{0.5})_xO_2$, $Sm_xNd_{0.15-x}Ce_{0.85}O_{2-\delta}$, $Ce_{0.7}Pr_xSm_yEu_{0.3-(x+y)}O_{2-\delta}$, CeO_2-$8Gd_2O_3$−$2Nd_2O_3$, and $Ce_{1-x}(Pr_{1/3}Sm_{1/3}Gd_{1/3})_xO_{2-\delta}$ and reported improved performance of ceria. Moreover, triple-doping or multi-doping in ceria has been studied and succeeded to improve the ionic conductivity of ceria [15–21]. However, further investigations are still required on tri- or multi-doped ceria in order to develop new electrolytes for future SOFC applications. In view of the above and based on DFT theory, recently, we have chosen the triple dopants, such as Pr^{3+} (59), Sm^{3+} (62), and Gd^{3+} (64), which are having an average atomic number about 61.67 (which is lies in between 61 and 62) and reported the studies on triple-doped ceria $Ce_{1-x}(Pr_{1/3}Sm_{1/3}Gd_{1/3})_xO_{2-\delta}$ system prepared via sol–gel auto-combustion route followed by conventional sintering at 1300 °C for 4 h. It has been found that the composition $Ce_{0.76}Pr_{0.08}Sm_{0.08}Gd_{0.08}O_{2-\delta}$ has the enhanced total ionic conductivity among the other compositions [17].

On the other hand, researchers have been focusing to reduce the sintering temperature and time with enhanced ionic conductivity. However, in the conventional sintering process, only sample surface retains the heat energy from the heating element in the furnace and by reducing the sintering temperature and time may decrease the relative density, which leads to lower ionic conductivity of a material. Therefore, researchers have been developing sintering techniques based on microwave energy, named as microwave sintering technique, which has gained much popularity compared to conventional sintering due to their less energy consumption, low sintering temperature, and time. Microwave sintering process facilitates the molecular-level rapid heating instead of surface-level conventional heating, which can enhance the density of the microstructure [22–26].

In the present paper, we have investigated the electrolyte material $Ce_{0.76}Pr_{0.08}Sm_{0.08}Gd_{0.08}O_{2-\delta}$ sintered by means of microwave sintering (1300 °C for 15, 30, and 60 min) and studied the effect of microwave sintering on structural, electrical, and thermal properties.

Experimental

The triple-doped ceria $Ce_{0.76}Pr_{0.08}Sm_{0.08}Gd_{0.08}O_{2-\delta}$ (PSG) as solid electrolyte material for IT-SOFC has been synthesized by adopting the sol–gel auto-combustion route. The starting materials for this synthesis have been taken in the form of nitrates, i.e., ceric ammonium nitrate ($Ce(NH_4)_2(NO_3)_6$), praseodymium (III) nitrate hexahydrate ($Pr(NO_3)_36H_2O$), samarium (III) nitrate hexahydrate ($Sm(NO_3)_36H_2O$), and gadolinium (III) nitrate hexahydrate ($Gd(NO_3)_36H_2O$). The detailed synthesis process has been discussed in our previous study reported elsewhere [17]. The final synthesized powder was calcined at 800 °C for 2 h. The obtained powder was then pressed into circular pellets at a pressure of 5 tons per square inch with the help of hydraulic press. The dense specimens have been obtained by sintering with a microwave furnace (microwave energy with 2.45 GHz) at 1300 °C for 15, 30, and 60 min, respectively. The nomenclature has been assigned to above said samples as PSG-MS15, PSG-MS30, and PSG-MS60.

The characterization of structural, electrical, and thermal properties of prepared triple-doped ceria electrolyte PSG materials has been carried out by powder X-ray diffraction (PXRD), scanning electron microscope (SEM), energy dispersive spectroscopy (EDS), Raman spectroscopy, impedance spectroscopy, and thermal expansion studies.

The powder X-ray diffraction at room temperature has been done with Philips Xpert PRO ALPHA1 Panalytical diffractometer using Cu Kα1 monochromatic radiation. The microstructure and elemental composition analyses of the sintered specimens have been carried out by SEM and EDS using ZEISS EVO 18 special edition. Sample formation and structural O_2-vacancy study of the samples have been done by Raman spectroscopy using a Horiba-Jobin Yvon micro-Raman spectrometer. The studies of impedance spectroscopy for all the samples in the temperature range from 200 to 600 °C have been carried out using Wayne Kerr impedance analyzer 6500B. The measurement of thermal expansion study has been done with Netzsch DIL 402 PC dilatometer from room temperature to 1000 °C.

Results and discussion

PXRD analysis

Figure 1 represents the PXRD patterns of all the microwave-sintered PSG-MS15, PSG-MS30, and PSG-MS60 samples. The PXRD patterns of all the samples reveal the formation of single phase with cubic-fluorite structure. The (hkl) parameters of all the samples indexed to (111), (200), (220), (311), (222), (400), (331), and (420) indicate the phase formation of compositions [$Fm\overline{3}m$ space group and JCPDS PDF: 34–0394]. Rietveld analysis was carried out for structural refinements of the PXRD patterns. The structural Rietveld refinements of all the samples were shown in Fig. 2. The straight line indicates that the difference between calculated and

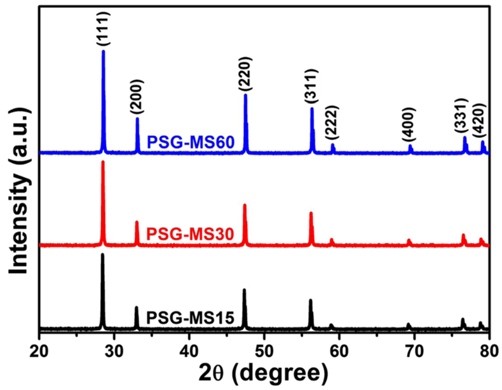

Fig. 1 PXRD patterns of PSG-MS15, PSG-MS30, and PSG-MS60

observed patterns is small. The structural refinement parameters were in good agreement, and lattice parameter values were calculated from the refinements of PXRD patterns and were listed in Table 1. Relative densities of all the samples were calculated from the equation below,

$$D_{\mathrm{rel}}(\%) = \frac{D_{\mathrm{m}}}{D_{\mathrm{th}}} \times 100 \tag{1}$$

where, “D_{rel}” is relative density, “D_{m}” is measured density measured by Archimedes principle, and “D_{th}” is theoretical density. The relative densities of all the PSG-MS15, PSG-MS30, and PSG-MS60 samples were found to be above 95% and were listed in Table 1. The Debye-Scherer equation was used to calculate the crystallite size (D) from PXRD patterns of the finely grounded sintered samples [17]. Table 1 represents the crystallographic data of prepared samples, i.e.,

Table 1 Crystallographic data of PSG-MS15, PSG-MS30, and PSG-MS60

Sample	PSG-MS15	PSG-MS30	PSG-MS60
Crystal structure	Cubic	Cubic	Cubic
Lattice parameter “a” (Å)	5.4252	5.4226	5.4104
Volume “V” (a^3)	159.67	159.45	158.38
Relative density (d/d_{th} %)	95.4	97.6	97.4
Crystallite size “D” (nm)	67	62	64
R_{p}	7.43	7.70	7.84
R_{wp}	10.30	10.2	10.6
R_{exp}	9.28	8.99	8.13
χ^2	1.24	1.28	1.71
Bragg R-factor	3.29	3.87	4.06
RF-factor	2.24	2.49	2.55
GOF	1.1	1.1	1.3

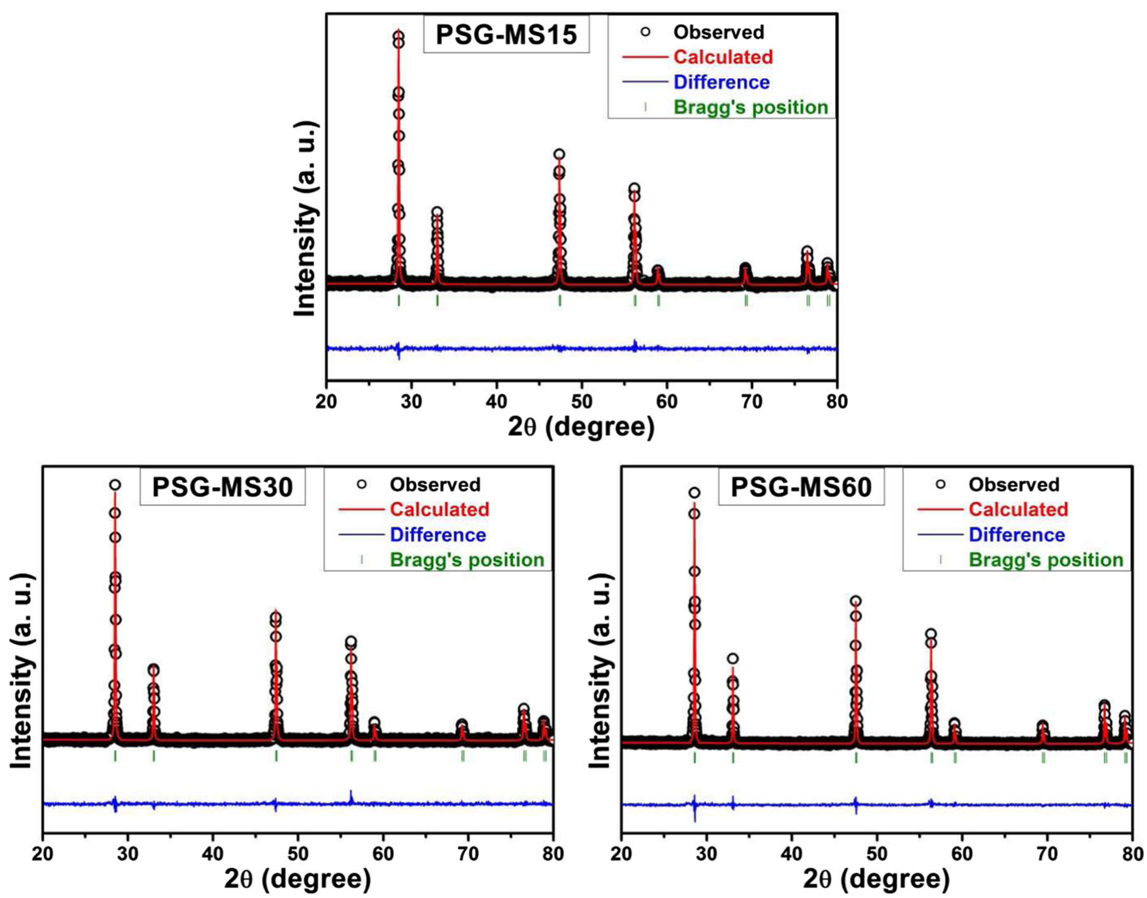

Fig. 2 Rietveld refinements of the PXRD patterns of PSG-MS15, PSG-MS30, and PSG-MS60

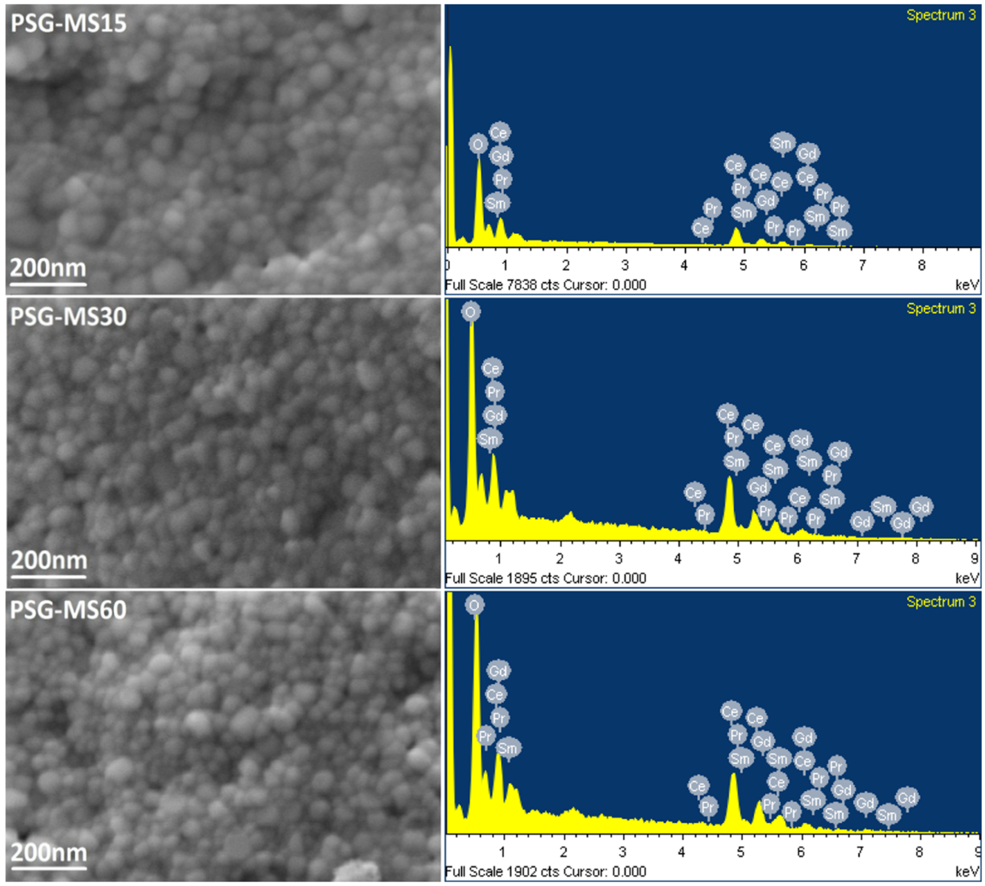

Fig. 3 SEM and EDS images of PSG-MS15, PSG-MS30, and PSG-MS60

crystal structure, lattice parameter, volume, relative density, and crystallite size for sintered samples, and Rietveld refinement parameters are R_p, R_{wp}, R_{exp}, χ^2, Bragg R-factor, RF factor, and goodness-of-fit (GOF).

SEM and EDS analyses

SEM micrographs of PSG-MS15, PSG-MS30, and PSG-MS60 specimens were shown in Fig. 3. In order to characterize the SEM analysis, prepared triple-doped ceria pellets were sputtered by Au coating. From Fig. 3, it can be observed that the grains were uniformly distributed in cluster-like form agglomeration and no large pores were observed on the surface of all samples. The calculated grain sizes at 248, 229, and 245 nm values were observed for PSG-MS15, PSG-MS30, and PSG-MS60, respectively. The EDS spectra of all the PSG-MS15, PSG-MS30, and PSG-MS60 specimens were shown in Fig. 3. Three selective regions of EDS spectra were analyzed for all the samples in order to observe the elemental composition. Presence of Ce, Pr, Sm, Gd, and O elements and the average percentage of elemental composition of all the samples were confirmed and listed in Table 2.

Table 2 Elemental composition analysis (EDS) of PSG-MS15, PSG-MS30, and PSG-MS60

Sample	Grain size (nm)	Atomic percentage of elements				
		Ce	Pr	Sm	Gd	O
PSG-MS15	248	25.38	2.70	2.71	2.69	66.52
PSG-MS30	229	25.36	2.72	2.74	2.73	66.45
PSG-MS60	245	25.35	2.72	2.69	2.74	66.50

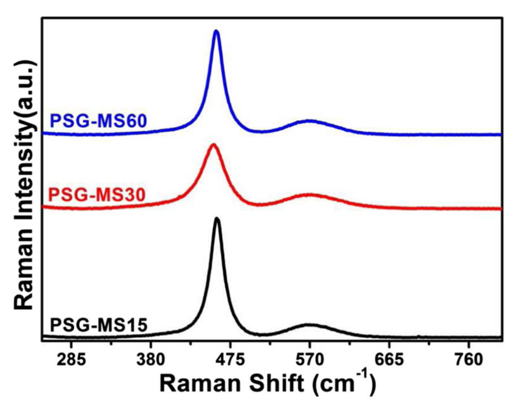

Fig. 4 Raman spectra of PSG-MS15, PSG-MS30, and PSG-MS60

Table 3 Raman analysis of PSG-MS15, PSG-MS30, and PSG-MS60

Sample	Raman analysis		
	$FWHM_{460}$ (cm^{-1})	I_{570}/I_{460}	A_{570}/A_{460}
PSG-MS15	19.21	0.12	0.37
PSG-MS30	29.82	0.24	0.56
PSG-MS60	19.91	0.15	0.48

Raman spectroscopy

Raman spectroscopy is a powerful tool to study the complete sample formation and oxygen vacancy confirmation in ceria-based solid electrolytes. Raman spectroscopy is an evidence for the electrical properties of ceria-based materials, i.e., the total ionic conductivity can be influenced by the structural oxygen vacancies in the ceria lattice [7, 9, 11, 27–31]. Figure 4 illustrates the Raman spectra for all the PSG-MS15, PSG-MS30, and PSG-MS60 samples. It can be observed from Fig. 4 that the Raman spectra of all the samples show two peaks: One intense peak centered at/around 460 cm^{-1}, which is assigned to the characteristic Raman mode of cerium ions surrounded with oxygen ions and confirms the formation of PSG-MS15, PSG-MS30, and PSG-MS60 solid electrolytes. Another peak positioned at/around 570 cm^{-1} is related to structural oxygen vacancies created in the solid solution due to triple doping with Pr^{3+}, Gd^{3+}, and Sm^{3+} in ceria [27–31]. Previously, it was reported that the concentration of structural oxygen vacancies in ceria-based electrolytes was estimated by (1) full-width half maxima of intense peak, i.e., $FWHM_{460}$; (2) intensity ratio of weak peak to the intense peak, i.e. I_{570}/I_{460}; and (3) area ratio of weak peak to the intense peak, i.e., A_{570}/A_{460} [29, 30].

Therefore, in the present study, we have made calculations on the full-width half maxima of intense peak, intensity ratio of weak and intense peak, and also the area ratio of weak and intense peaks for the entire microwave-sintered PSG-MS15, PSG-MS30, and PSG-MS60 samples and were presented in Table 3. It is found that the PSG-MS30 shows the high value of full-width half maxima ($FWHM_{460}$), intensity ratio (I_{570}/I_{460}), as well as area ratio (A_{570}/A_{460}), which indicates the high concentration of oxygen vacancies in the composition over others.

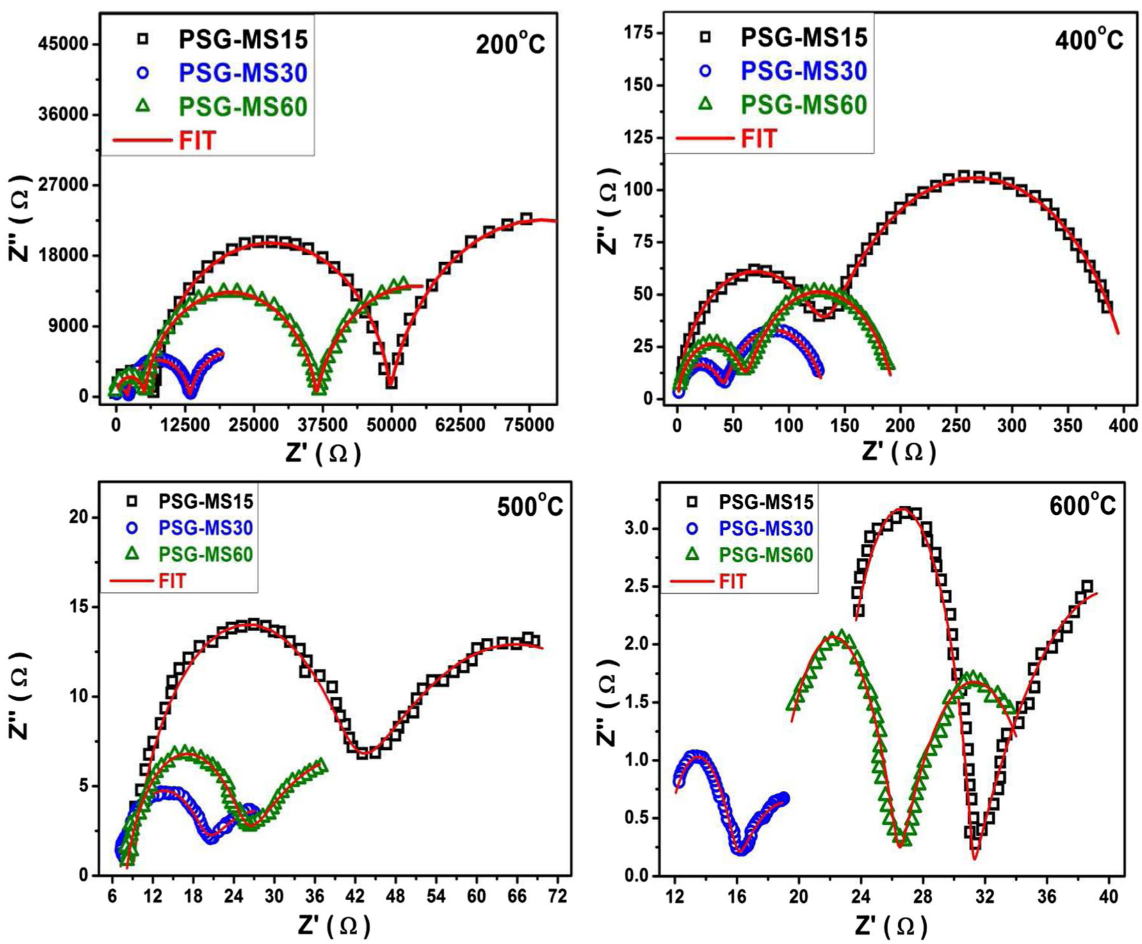

Fig. 5 Fitted complex impedance plots of PSG-MS15, PSG-MS30, and PSG-MS60

Table 4 Fitting results of the complex impedance plots for PSG-MS15, PSG-MS30, and PSG-MS60

Sample	Temp. (°C)	R_g (Ω)	CPE-T (nF)	CPE-P	R_{gb} (Ω)	CPE-T (μF)	CPE-P	R_t (Ω)
PSG-MS15	200	6469	0.198	0.99	43,220	0.162	0.94	49,689
	400	129	97.4	0.92	279	9.924	0.82	408
PSG-MS30	200	2022	0.451	0.97	11,356	0.375	0.88	13,378
	400	46	467.2	0.84	87	67.45	0.79	133
PSG-MS60	200	5077	0.149	0.99	31,287	0.098	0.90	36,364
	400	61	175.4	0.89	134	24.58	0.83	195

Due to the highly concentrated structural oxygen vacancies of microwave-sintered PSG-MS30 sample, one may expect higher total ionic conductivity for the PSG-MS30 sample.

Electrical analysis

The electrical properties of triple-doped ceria solid electrolytes were analyzed by a well-established tool, i.e., impedance spectroscopy. Generally, impedance spectra, i.e., complex impedance spectra is a plot of the real part of the impedance (Z') and imaginary part of impedance ($-Z''$) and is a characteristic nature of the conducting material. The complex impedance spectra have three successive contributions in different frequency regions, such as electrode contribution that corresponds to lower frequency region, grain boundary contribution to a moderate frequency region, and grain/bulk contribution to a higher frequency region [9, 10, 32, 33]. The complex impedance plots of all the sintered samples at 200 and 400 °C were presented in Fig. 5, and the three distinguishable semicircles correspond to grain, grain boundary, and electrode processes. Further, it is confirmed that the increase in temperature decreases the resistance of grain and grain boundary. Z-View software is used to fit the complex impedance plots with an equivalent circuit, which consists of the combination of resistances (R) and constant phase elements (CPE). Fitting results of the complex impedance plots for PSG-MS15, PSG-MS30, and PSG-MS60 samples were listed in Table 4. The grain resistance is represented by "R_g," the grain boundary resistance is represented by "R_{gb}," and the total resistance is calculated from the grain and grain boundary resistances, which is represented by "R_t" ($R_t = R_g + R_{gb}$). The total resistance, i.e., the sum of grain resistance and grain boundary resistance was taken into account to calculate the total ionic conductivity (σ_t) of all the specimens using the following equation:

$$\sigma_t = \frac{l}{R_t A} \tag{2}$$

where, "l" is the thickness of the sample and "A" is collected electrode area. The calculated total ionic conductivity values for PSG-MS15, PSG-MS30, and PSG-MS60 samples were presented in Table 5. The highest total ionic conductivity was observed for PSG-MS30 (3.47×10^{-2} S cm^{-1}) as compared to PSG-MS15 and PSG-MS60 samples. The high value of total ionic conductivity is because of the fast migration of ions in the prepared triple-doped ceria solid solution due to the formation of concentrated oxygen vacancies in the material. The Raman spectroscopy is an evidence for the formation of high concentrated oxygen vacancies, which were analyzed by calculating the 460_{FWHM}, I_{570}/I_{460}, and A_{570}/A_{460}. The comparison has been made for the total ionic conductivity of present optimized microwave-sintered sample with recently studied different samples, such as single-doped, double-doped and triple/multi-doped ceria samples via different sintering techniques presented in Table 6.

To calculate the activation energy for conduction, the logarithm of total ionic conductivity with the inverse of the temperature (i.e., log (σT) v/s 1000/T) was plotted using Arrhenius relation,

$$\sigma T = \sigma_0 \exp\left(-\frac{E_a}{KT}\right) \tag{3}$$

where, "E_a" represents the activation energy for conduction, "T" denotes the absolute temperature, "K" indicates

Table 5 Total ionic conductivities and activation energies of PSG-MS15, PSG-MS30, and PSG-MS60

Sample	Conductivity "σ_t" (S cm^{-1})		Activation energies			
	At 500 °C	At 600 °C	E_a^{g} (eV)	E_a^{gb} (eV)	E_a^{t} (eV)	E_a^{t} (eV) (≥450 °C)
PSG-MS15	0.0048	0.0147	0.70	0.77	0.73	0.68
PSG-MS30	0.0134	0.0347	0.64	0.72	0.69	0.56
PSG-MS60	0.0081	0.022	0.67	0.75	0.71	0.61

Table 6 Comparison study of total ionic conductivity for PSG-MS30

Sample	Sintering type	Sintering temp.–time	Conductivity σ_t (S/cm)	Activation energy (eV)	Reference
PSG-MS30	Microwave	1300 °C–30 min	0.0347 at 600 °C	0.69	Present
$Ce_{0.76}Pr_{0.08}Sm_{0.08}Gd_{0.08}O_{2-\delta}$	Conventional	1300 °C–4 h	0.0186 at 600 °C	0.56	[17]
$Ce_{0.84}Gd_{0.08}Pr_{0.08}O_2$	Conventional	1300 °C–10 h	0.0171 at 600 °C	0.77	[10]
$Ce_{0.8}Sm_{0.12}Pr_{0.08}O_{2-\delta}$	Conventional	1300 °C–10 h	0.0121 at 600 °C	0.77	[11]
$Ce_{0.85}Gd_{0.1}Sm_{0.05}O_{1.925}$	Conventional	1500 °C–14 h	0.046 at 700 °C	–	[12]
$Ce_{0.7}Pr_{0.15}Sm_{0.075}Eu_{0.075}O_{2-\delta}$	Conventional	600 °C–6 h	0.0003 at 500 °C	0.39	[15]
$Ce_{0.8}Sm_{0.18}Ca_{0.02}O_{2-\delta}$	Microwave	1450 °C–30 min	0.0018 at 500 °C	0.82–1.06	[23]
$Ce_{0.8}Yb_{0.2}O_{1.9}$	Microwave	1500 °C–15 min	0.013 at 800 °C	1.07	[24]
$Ce_{1-x}Bi_xO_{2-\delta}$	Microwave	1050 °C–1 h	0.0002 at 600 °C	–	[25]

the Boltzmann constant, and "σ_0" is the pre-exponential factor.

Figure 6a–c shows the grain, grain boundary, and total ionic conductivity of all the samples presented in the form of Arrhenius relation within the temperature range of 200 and 600 °C. The activation energies of all the PSG-MS15, PSG-MS30, and PSG-MS60 samples were then calculated from the linearized Arrhenius plots. From Fig. 6c at/above 450 °C, it can be observed that there is a slight slope change in Arrhenius plots incorporated as an inset in Fig. 6c. This is due to the presence of distinct activation energies in the form of association enthalpy and migration enthalpy. The vacancy associated with the cerium cation is trapped; results in activation energy in the form of association enthalpy and the free migration of oxygen vacancies in the lattice results in activation energy in the form of migration enthalpy. In the low-temperature region, the activation energy is the sum of association and migration enthalpies, whereas in the high temperature region, only migration enthalpy contributes to the activation energy [10]. Therefore, at higher temperatures (≥ 450 °C), the free migration of concentrated oxygen vacancies results in activation energy in the form of migrated enthalpy and leads to changes in the slope. It is observed from Fig. 6 that the change in the slopes results in a change in the activation energies for all the samples and the activation energy values were listed in Table 5. The presence of mobile oxygen

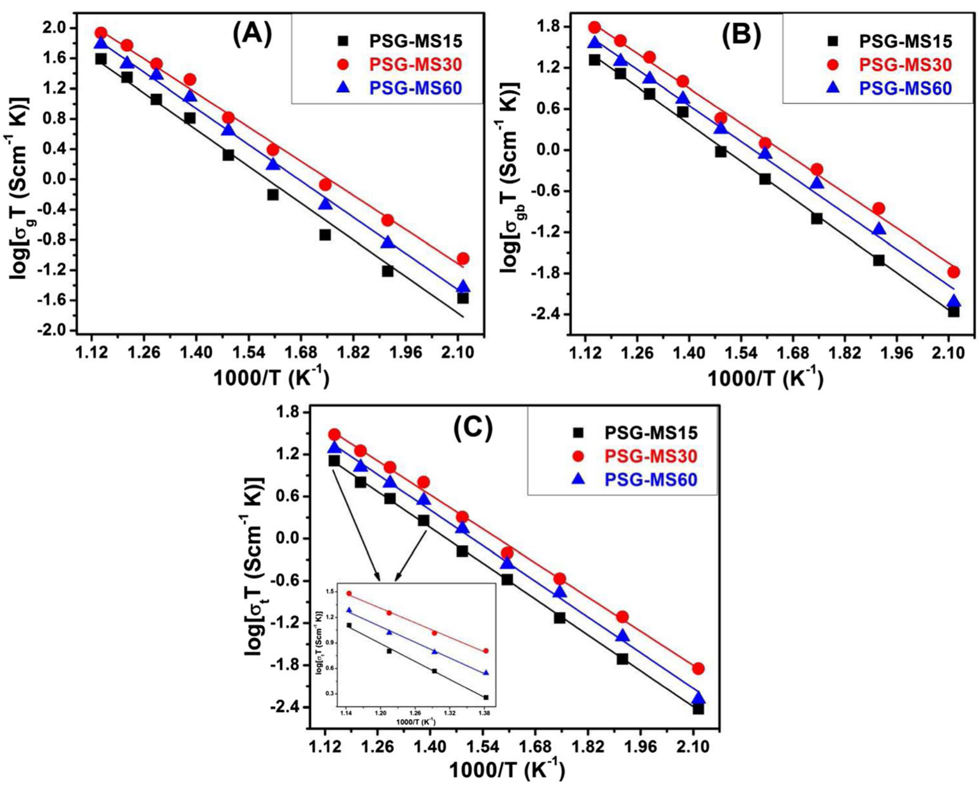

Fig. 6 Arrhenius plots for grain (**a**), grain boundary (**b**), and total ionic conductivity (**c**) of PSG-MS15, PSG-MS30, and PSG-MS60

vacancies (defects) and interaction between dopant ions and vacancies leads to the low activation energy for microwave-sintered PSG-MS30 sample (i.e., 0.69 eV) [34].

From the above discussions, as the sintering time is increased, it can be concluded that (1) the density of the samples increased up to 30 min then slightly decreased for 60 min and (2) the grain size becomes fine up to 30 min and then increased for 60 min. A finer grain size with uniform dense microstructure will result in lower activation energy, i.e., more oxygen vacancies in the composition were observed for the PSG-MS30 composition [7, 23, 25, 26]. Lowest activation energy indicating the presence of free migrated oxygen vacancies in the composition leads to enhanced highest total ionic conductivity of the sample. In addition to this, the concentration of oxygen vacancies with the sintering time was studied and estimated using Raman analysis (Table 3), and the high concentration of oxygen vacancies of PSG-MS30 composition is responsible for the enhanced ionic conductivity [26, 29, 30].

Thermal expansion analysis

Thermal expansion analysis of a ceria-based material plays an important role in IT-SOFC applications. To sustain ceria as solid electrolyte for IT-SOFC, in addition to structural and electrical properties, it must have matched thermal expansion coefficient with the other components of a SOFC. The moderate, comparable thermal expansion coefficient of cell modules avoids the mismatch/μ-cracks between them [34, 35]. In view of the above, we have made measurement of thermal expansion for PSG-MS30 sample in the temperature range from room temperature to 1000 °C. The temperature-dependent linear thermal expansion (dL/dL_0) curve for the PSG-MS30 sample was presented in Fig. 7. The thermal expansion coefficient (TEC) was then calculated from the curve of linear thermal expansion by the following equation:

$$\mathrm{TEC} = \frac{(\mathrm{L}-\mathrm{L}_0)/\mathrm{L}_0}{\mathrm{T}-\mathrm{T}_0} \quad (4)$$

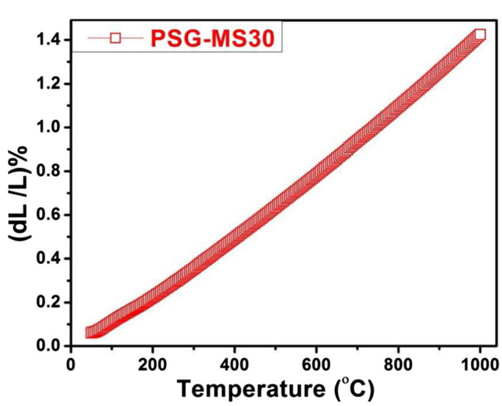

Fig. 7 Temperature-dependent thermal expansion curve for PSG-MS30

where "L_0" is the initial and "L" is the final lengths of the specimen, "T_0" is the start and "T" is the end temperatures of the measurement. It is observed that the TEC value of PSG-MS30 sample (13.43×10^{-6} °C^{-1} for 30–800 °C and 14.02×10^{-6} °C^{-1} for 30–1000 °C) shows good thermal compatibility with the reported electrolyte and electrode materials, like $Ce_{0.76}Sm_{0.2}Pr_{0.04}O_{2-\delta}$ electrolyte (13.31×10^{-6} °C^{-1} for 30–800 °C and 13.78×10^{-6} °C^{-1} for 30–1000 °C), $La_{0.6}Sr_{1.4}MnO_4$ anode (14.15×10^{-6} °C^{-1} for 30–1000 °C) and $Ba_{0.6}Sr_{0.4}Co_{0.9}Nb_{0.1}O_{3-\delta}$–(20%)$Gd_{0.1}Ce_{0.9}O_{1.95}$composite cathode ($14.90 \times 10^{-6}$ °C^{-1} for 30–1000 °C) [9, 35–41].

Conclusions

The $Ce_{0.76}Pr_{0.08}Sm_{0.08}Gd_{0.08}O_{2-\delta}$ (PSG) material as solid electrolyte for IT-SOFCs has been successfully synthesized by sol–gel auto-combustion route. The effect of microwave sintering on structural, electrical, and thermal properties of prepared electrolyte material was studied and compared. PXRD analysis revealed the single-phase confirmation of all the samples with cubic fluorite structure. SEM and EDS analyses revealed the dense microstructure and distribution of elemental analysis for all the samples. Microwave sintering resulted in improved electrical properties of the sample which is evidenced by the concentration of oxygen vacancies evaluated from Raman analysis. The highest total ionic conductivity, i.e., 3.47×10^{-2} S cm^{-1} at 600 °C with minimum activation energy of 0.69 eV, is observed for microwave-sintered PSG-MS30 sample when compared to PSG-MS15 and PSG-MS60. The moderate value of coefficient of thermal expansion, 14.02×10^{-6} °C^{-1}, is observed for the PSG-MS30 sample. The highest total ionic conductivity with minimum activation energy and moderate thermal expansion coefficient of microwave-sintered PSG-MS30 sample makes the possibility of its use as solid electrolyte in IT-SOFC applications.

Acknowledgements One of the authors, Kasarapu Venkataramana, thanks the University Grants Commission (UGC), New Delhi, India, for the financial assistance under the scheme of the UGC-UPE-FAR program.

References

1. Stambouli B, Traversa E (2002) Solid oxide fuel cells (SOFCs): a review of an environmentally clean and efficient source of energy. Renew Sust Energ Rev 6(5):433–455. https://doi.org/10.1016/S1364-0321(02)00014-X
2. Minh NQ (1993) Ceramic Fuel Cells. J Am Ceramic Soc 76(3): 563–588. https://doi.org/10.1111/j.1151-2916.1993.tb03645.x
3. Inaba H, Tagawa H (1996) Ceria-based solid electrolytes. Solid State Ionics 83(1-2):1–16. https://doi.org/10.1016/0167-2738(95)00229-4

4. Bhabu KA, Theerthagiri J, Madhavan J, Balu T, Muralidharan G, Rajasekaran TR (2016) Cubic fluorite phase of samarium doped cerium oxide $(CeO_2)_{0.96}Sm_{0.04}$ for solid oxide fuel cell electrolyte. J Mater Sci Mater Electron 27(2):1566–1573. https://doi.org/10.1007/s10854-015-3925-z
5. Ahmed SI, Mohammed T, Bahafi A, Suresh MB (2017) Effect of Mg doping and sintering temperature on structural and morphological properties of samarium-doped ceria for IT-SOFC electrolyte. Appl Nanosci 7(5):243–252. https://doi.org/10.1007/s13204-017-0567-x
6. Dikmen S, Aslanbay H, Dikmen E, Sahin O (2010) Hydrothermal preparation and electrochemical properties of Gd^{3+} and Bi^{3+}, Sm^{3+}, La^{3+}, and Nd^{3+}codoped ceria-based electrolytes for intermediate temperature-solid oxide fuel cell. J Power Sources 195(9):2488–2495. https://doi.org/10.1016/j.jpowsour.2009.11.077
7. Tadokoro SK, Muccillo ENS (2007) Effect of Y and Dy co-doping on electrical conductivity of ceria ceramics. J Eur Ceramic Soc 27(13-15):4261–4264. https://doi.org/10.1016/j.jeurceramsoc.2007.02.138
8. Pikalova EY, Murashkina AA, Maragou VI, Demin AK, Strekalovsky VN, Tsiakaras PE (2011) CeO_2 based materials doped with lanthanides for applications in intermediate temperature electrochemical devices. Int J Hydrog Energy 36(10):6175–6183. https://doi.org/10.1016/j.ijhydene.2011.01.132
9. Ji B, Tian C, Wang C, Wu T, Xie J, Li M (2015) Preparation and characterization of $Ce_{0.8}Y_{0.2-x}Cu_xO_{2-\delta}$ as electrolyte for intermediate temperature solid oxide fuel cells. J Power Sources 278:420–429. https://doi.org/10.1016/j.jpowsour.2014.12.073
10. Ramesh S, James Raju KC (2012) Preparation and characterization of $Ce_{1-x}(Gd_{0.5}Pr_{0.5})_xO_2$ electrolyte for IT-SOFCs. Int J Hydrog Energy 37(13):10311–10317. https://doi.org/10.1016/j.ijhydene.2012.04.008
11. Xiaomin L, Qiuyue L, Lili Z, Xiaomei L (2015) Synthesis and characterization of $Ce_{0.8}Sm_{0.2-x}Pr_xO_{2-\delta}$ (x = 0.02–0.08) solid electrolyte materials. J Rare Earths 33(4):411–416. https://doi.org/10.1016/S1002-0721(14)60434-8
12. Wang FY, Wan BZ, Cheng S (2005) Study on Gd^{3+} and Sm^{3+} co-doped ceria electrolytes. J Solid State Electrochem 9(3):168–173. https://doi.org/10.1007/s10008-004-0575-0
13. Anderson DA, Simak SI, Skorodumova NV, Abrikosov IA, Johansson B (2006) Optimization of ionic conductivity in doped ceria. PANS 103:3518–3521. https://doi.org/10.1073/pnas.0509537103
14. Rai A, Mehta P, Omar S (2014) Conduction behavior in $Sm_xNd_{0.15-x}Ce_{0.85}O_{2-\delta}$. Solid State Ionics 263:190–196. https://doi.org/10.1016/j.ssi.2014.06.009
15. Anirban S, Dutta A (2016) Microstructure and charge carrier dynamics in Pr-Sm-Eu triple-doped nanoceria. Solid State Ionics 295:48–56. https://doi.org/10.1016/j.ssi.2016.07.008
16. Babu AS, Bauri R, Srinivas Reddy G (2016) Processing and conduction behavior of nanocrystalline Gd-doped and rare earth co-doped ceria electrolytes. Electrochim Acta 209:541–550. https://doi.org/10.1016/j.electacta.2016.05.118
17. Venkataramana K, Madhuri C, Suresh Reddy Y, Bhikshamaiah G, Vishnuvardhan Reddy C (2017) Structural, electrical and thermal expansion studies of tri-doped ceria electrolyte materials for IT-SOFCs. J. Alloys Compd 719:97–107. https://doi.org/10.1016/j.jalcom.2017.05.022
18. Boskovic S, Zec S, Brankovic G, Brankovic Z, Devecerski A, Matovic B, Aldinger F (2010) Preparation, sintering and electrical properties of nano-grained multi doped ceria. Ceram Int 36(1):121–127. https://doi.org/10.1016/j.ceramint.2009.07.015
19. Stojmenovic M, Boskovic S, Bucevac D, Prekajski M, Babic B, Matovic B (2013) Electrical characterization of multi doped ceria ceramics. Ceram Int 39(2):1249–1255. https://doi.org/10.1016/j.ceramint.2012.07.055
20. Stojmenovic M, Boskovic S, Zunic M, Varela JA, Prekajski M, Matovic B, Mentus S (2014) Electrical properties of multi doped ceria. Ceram Int 40(7):9285–9292. https://doi.org/10.1016/j.ceramint.2014.01.151
21. Muhammed Ali SA, Anwar M, Abdalla AM, Somalu MR, Muchtar A (2017) $Ce_{0.80}Sm_{0.10}Ba_{0.05}Er_{0.05}O_{2-\delta}$ multi-doped ceria electrolyte for intermediate temperature solid oxide fuel cells. Ceram Int 43(1):1265–1271. https://doi.org/10.1016/j.ceramint.2016.10.075
22. Oghbaei M, Mirzae O (2010) Microwave versus conventional sintering: a review of fundamentals, advantages and applications. J Alloys Compounds 494(1-2):175–189. https://doi.org/10.1016/j.jallcom.2010.01.068
23. Gonjal JP, Heuguet R, Gil DM, Calzada AR, Marinel S, Moran E, Schmidt R (2015) Microwave synthesis & sintering of Sm and Ca co-doped ceria ceramics. Int J Hydrog Energy 40(45):15640–15651. https://doi.org/10.1016/j.ijhydene.2015.07.161
24. Cesario MR, Savary E, Marinel S, Raveau B, Caignaert V (2016) Synthesis and electrochemical performance of $Ce_{1-x}Yb_xO_{2-x/2}$ solid electrolytes: the potential of microwave sintering. Solid State Ionics 294:67–72. https://doi.org/10.1016/j.ssi.2016.07.005
25. Prekajski M, Stojmenovic M, Radojkovic A, Brankovic G, Oraon H, Subasri R, Matovic B (2014) Sintering and electrical properties of $Ce_{1-x}Bi_xO_{2-\delta}$ solid solution. J Alloys Compounds 617:563–568. https://doi.org/10.1016/j.jallcom.2014.08.090
26. Venkataramana K, Ravindranath K, Madhuri C, Madhusudan C, Kumar NP, Reddy CV (2017) Low temperature microwave sintering of yttrium and samarium co-doped ceria solid electrolytes for IT-SOFCs. Ionics. https://doi.org/10.1007/s11581-017-2293-5
27. Askrabic A, Dohcevic-Mitrovic ZD, Radovic M, scepanovic M, Popovic ZV (2009) Phonon-phonon interactions in $Ce_{0.85}Gd_{0.15}O_{2-\delta}$ nanocrystals studied by Raman spectroscopy. J Raman Spectrosc 40(6):650–655. https://doi.org/10.1002/jrs.2177
28. Peng C, Wang Y, Jiang K, Bin BQ, Liang HW, Feng J, Meng J (2003) Study on the structure change and oxygen vacation shift for $Ce_{1-x}Sm_xO_{2-\delta}$ solid solution. J Alloys Compounds 349(1-2):273–278. https://doi.org/10.1016/S0925-8388(02)00903-9
29. Li SP, Lu JQ, Fang P, Luo MF (2009) Effect of oxygen vacancies on electrical properties of $Ce_{0.8}Sm_{0.1}Nd_{0.1}O_{2-\delta}$ electrolyte: an in situ Raman spectroscopic study. J Power Sources 193(1):93–98. https://doi.org/10.1016/j.jpowsour.2008.12.022
30. López JM, Gilbank AL, García T, Solsona B, Agouram S, Torrente-Murciano L (2015) The prevalence of surface oxygen vacancies over the mobility of bulk oxygen in nanostructured ceria for the total toluene oxidation. Appl Catal B Environ 174–175:403–412. https://doi.org/10.1016/j.apcatb.2015.03.017
31. Stojmenovic M, Boskovic S, Zunic M, Bbic B, Matovic B, Bajuk-Bogdanovic D, Mentus S (2015) Studies on structural, morphological and electrical properties of $Ce_{1-x}Er_xO_{2-\delta}$ (x = 0.05–0.20) as solid electrolyte for IT-SOFC. Mater Chem Phys 153:422–431. https://doi.org/10.1016/j.matchemphys.2015.01.036
32. Anjaneya KC, Nayaka GP, Manjanna J, Govindaraj G, Ganesha KN (2013) Preparation and characterization of $Ce_{1-x}Gd_xO_{2-\delta}$ (x = 0.1–0.3) as solid electrolyte for intermediate temperature SOFC. J Alloys Compounds 578:53–59. https://doi.org/10.1016/j.jallcom.2013.05.010
33. Wu YC, Lin CC (2014) The microstructures and property analysis of aliovalent cations (Sm^{3+}, Mg^{2+}, Ca^{2+}, Sr^{2+}, Ba^{2+}) co-doped ceria-based electrolytes after aging treatment. Int J Hydrog Energy 39(15):7988–8001. https://doi.org/10.1016/j.ijhydene.2014.03.063
34. Ramesh S, Kumar VP, Kistaiah P, Reddy CV (2010) Preparation, characterization and thermo electrical properties of co-doped $Ce_{0.8-x}Sm_{0.2}Ca_xO_{2-\delta}$ materials. Solid State Ionics 181(1-2):86–91. https://doi.org/10.1016/j.ssi.2009.11.014
35. Prashanth Kumar V, Reddy YS (2008) Thermal and electrical properties of rare-earth co-doped ceria ceramics. Mater Chem Phys

112(2):711–718. https://doi.org/10.1016/j.matchemphys.2008.06.030

36. Tian C, Ji B, Xie J, Bao W, Liu K, Cheng J, Yin Q (2014) Preparation and characterization of $Ce_{0.8}La_{0.2-x}Y_xO_{1.9}$ as electrolyte for solid oxide fuel cells. J Rare Earths 32(12):1162–1169. https://doi.org/10.1016/S1002-0721(14)60198-8
37. Venkatesh V, Prashanth Kumar V, Sayanna R, Vishnuvardhan Reddy C (2012) Preparation, characterization and thermal expansion of Pr co-dopant in samarium doped ceria. Adv Mater Phys Chem 2(04):5–8. https://doi.org/10.4236/ampc.2012.24B002
38. Jin C, Yang Z, Zhang H, Yang C, Chen F (2012) $La_{0.6}Sr_{1.4}MnO_4$ layered perovskite anode material for intermediate temperature solid oxide fuel cells. Electrochem Comm 14(1):75–77. https://doi.org/10.1016/j.elecom.2011.11.008
39. Yaremchenko AA, Brinkmann B, Janssen R, Frade JR (2013) Electrical conductivity, thermal expansion and stability of Y- and Al-substituted $SrVO_3$ as prospective SOFC anode material. Solid State Ionics 247-248:86–93. https://doi.org/10.1016/j.ssi.2013.06.002
40. Kong X, Sun H, Yi Z, Wang B, Zhang G, Liu G (2017) Manganese-rich $SmBaCo_{2-x-y}Mn_xMg_yO_{5+\delta}$ (x = 0.5, 1, 11.5 and y = 0.05, 0.1) with stable structure and low thermal expansion coefficient as cathode materials for IT-SOFCs. Ceram Int 43(16):13394–13400. https://doi.org/10.1016/j.ceramint.2017.07.042
41. Zhang L, Liu M, Huang J, Song Z (2014) Improved thermal expansion and electrochemical performances of $Ba_{0.6}Sr_{0.4}Co_{0.9}Nb_{0.1}O_{3-\delta}$–$Gd_{0.1}Ce_{0.9}O_{1.95}$ composite cathodes for IT-SOFCs. Int J Hydrog Energy 39(15):7972–7979. https://doi.org/10.1016/j.ijhydene.2014.03.055